




Cite this: *RSC Appl. Interfaces*, 2024,  
1, 323

# All slot-die coated organic solar cells using an amine processed cathode interlayer based upon an amino acid functionalised perylene bisimide†

Rebecca E. Ginesi, <sup>a</sup> Muhammad R. Niazi,<sup>b</sup>  
Gregory C. Welch <sup>\*b</sup> and Emily R. Draper <sup>\*a</sup>

Green solution-processable organic photovoltaic cells (OPVs) have the potential to provide low-cost, clean, and accessible electricity. However, there are few organic materials that are compatible with multi-layer film formatting from halogen-free solvents using scalable coating methods. Current research focuses on devices using tin oxide (SnO<sub>2</sub>). However, SnO<sub>2</sub> has surface traps and requires a passivating layer to maximise performance. Therefore, it is crucial to develop electron deficient organic materials that can passivate metal oxides to achieve maximum device performance. Rendering these materials and films solvent resistance is thus a major goal. Herein, we show that SnO<sub>2</sub> modified with a tyrosine appended perylene bisimide (PBI-Y) can be applied as an electron transport interlayer in PM6/Y6C12-based organic photovoltaic cells using an amine-based ink formulation. The SnO<sub>2</sub>/PBI-Y films are characterised by optical absorption spectroscopy and atomic force microscopy and exhibit solvent resistance. The electrical characterisation shows that a PBI modification improves the conductivity of the SnO<sub>2</sub>. Spin-coated devices show a power conversion efficiency (PCE) of 13%, among the best for all air-processed SnO<sub>2</sub>-based OPVs. Fully slot-die coated devices achieve PCEs of 10%, demonstrating the potential for scale-up. This work opens a viable and sustainable method to develop organic photovoltaic devices using more environmentally friendly processing conditions.

Received 28th September 2023,  
Accepted 3rd December 2023

DOI: 10.1039/d3lf00183k

rsc.li/RSCApplInter

## Introduction

Solution-processed organic photovoltaic cells (OPVs) are considered one of the most promising next-generation, low-cost, clean energy technologies.<sup>1–4</sup> Compared to the more traditional silicon-based solar cells, OPVs can be rendered lightweight, flexible, and stretchable, allowing them to be integrated onto large-area flat, curved, or flexible surfaces.<sup>5–8</sup> Furthermore, lab-scale OPV devices with power conversion efficiencies (PCEs) of up to 18% have been reported, which paves the way for future commercialisation.<sup>9–11</sup> However, further work to improve performance, lifetime, and processing is needed for this technology to become widespread in commercial applications.

Many high-performing OPVs currently are made using spin-coating methods inside gloveboxes,<sup>12</sup> and processing conditions and performance metrics are often not transferable

to industry-scale fabrication methods. The use of non-environmentally friendly halogenated solvents, such as chlorobenzene (most commonly used to cast photoactive layer films), also presents challenges due to the health and environmental impacts associated with such solvents.<sup>13</sup> Therefore, a potential solution is to use large-scale coating techniques, such as slot-die coating,<sup>14–16</sup> with green solvents (*i.e.*, solvents which are more environmentally friendly, are usually made from renewable resources, have a lower toxicity and are biodegradable)<sup>17</sup> at the lab-scale to facilitate more rapid adoption of new innovations. Slot-die coating allows for highly reproducible uniform films, low material wastage, and can be compatible with roll-to-roll (R2R) processing technology, allowing for high throughput.<sup>18,19</sup> Recently, all slot-die coated OPVs with a record PCE of 16.2% have been reported.<sup>20</sup>

The electron transport layer (ETL) plays a crucial role in the PCE, stability and reliability of solar cells.<sup>21</sup> OPVs with conducting transparent n-type metal oxides, such as tin oxide (SnO<sub>2</sub>) and zinc oxide (ZnO), are commonly observed in consumer electronics, such as in touch screen panels, smart windows, and energy storage devices.<sup>22–25</sup> However, ZnO can promote the photodegradation of bulk heterojunction (BHJ) materials, negatively impacting device performance.<sup>26</sup> Therefore, SnO<sub>2</sub> is the more viable choice owing to its higher

<sup>a</sup> School of Chemistry, University of Glasgow, Glasgow G12 8QQ, UK.

E-mail: emily.draper@glasgow.ac.uk

<sup>b</sup> Department of Chemistry, University of Calgary, Calgary, Alberta T2N 1N6, Canada† Electronic supplementary information (ESI) available. See DOI: <https://doi.org/10.1039/d3lf00183k>

conductivity, transparency in the visible region, less absorption in the ultraviolet region, and wider bandgap to block holes effectively.<sup>27</sup> Furthermore, SnO<sub>2</sub> does not require activation by light. However, the solution-based fabrication process can result in surface defects, and thus, there is great interest in modifying the surface of SnO<sub>2</sub> using organic materials. An area of focus is developing bottom organic interlayers (for inverted-type devices) that are necessary for improving device performance but can withstand the coating of photoactive materials on top with solvents commonly used to dissolve organics, such as aromatics and furans.

Over the past few years, there have been intensive studies focused on surface-modified SnO<sub>2</sub>-ETLs using organic molecules as cathode interlayers (Fig. 1). Several materials have been investigated, including quantum dots,<sup>28</sup> conjugated polymers,<sup>29</sup> and organic small molecules.<sup>30</sup> Perylene bisimide (PBI) derivatives, also known as perylene diimides (PDIs), have high electron mobility, strong absorption, and high thermal stability, making them attractive candidates as ETLs in OPV devices.<sup>31,32</sup>

Munir *et al.* have previously reported OPV devices based on an N-annulated PDI with a functional N-H bond (PDIN-H) for indoor and outdoor use.<sup>33</sup> The devices gave an improved PCE of 9.19% (compared to 1.52% for SnO<sub>2</sub> alone) and a fill factor of 56% after treatment of the SnO<sub>2</sub> layer with UV-ozone. However, PDIN-H is an insoluble material due to intermolecular CO-NH hydrogen bonding, and thus requests a protection/deprotection strategy for efficient green solvent processing.<sup>33</sup> If PBIs are functionalised with amino acids, they have increased solubility in solvents such as water due to deprotonation of the terminal carboxylic acids.<sup>31,34</sup> We have reported aqueous solution deposited ETLs using amino acid functionalised PBIs on top of ZnO.<sup>35</sup> Devices gave good PCEs of 2.55% using P3HT-based photoactive layers. However, these solutions were prepared using 1 equivalent of NaOH (0.1 M, aq), which is a corrosive base and not ideal for large-scale module manufacturing. Thus, there is immediate interest in developing green solvent systems to make these films.

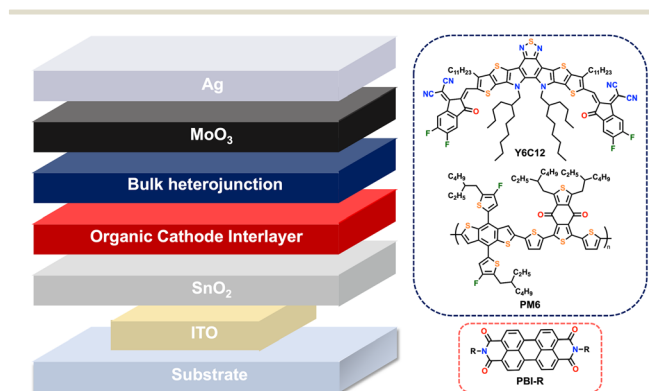


Fig. 1 3D device architecture of an organic photovoltaic cell, and examples of the organic cathode interlayer (red dashed box) and bulk heterojunction layer (blue dashed box) used in the devices discussed in this paper.

Herein, we use a perylene bisimide appended with L-tyrosine (**PBI-Y**) and a volatile amine base (butylamine) to create an ink used to coat and modify SnO<sub>2</sub> films for use in OPV devices. We report devices fabricated under ambient conditions, in air, using spin-coating and slot-die coating techniques, to obtain PCEs of 9–13%, among the best reported. The **PBI-Y** films showed solvent resistance upon exposure to water, *o*-xylene and ethanol, allowing for the successful demonstration of scalable, multi-layer planar OPVs. Atomic force microscopy (AFM) images of spin-coated and slot-die coated films showed similar smooth features in the presence of **PBI-Y**. The results indicate that amino acid functionalised PBIs can be processed from green solvent systems and applied as cathode interlayers (CILs) in high-performance, low-cost industrial OPVs.

## Results and discussion

### Materials selection and green solvent processing

PBIs appended with amino acids can be easily synthesised on a large scale.<sup>36</sup> These PBIs can be rendered soluble upon the addition of a base, such as butylamine, allowing the use of green solvents during device fabrication (Fig. 2). Butylamine was chosen as it is basic enough to deprotonate the amino acid, has a suitable vapor pressure to allow for large area slot-die coated films, and is considered green. We first screened a series of amino acid functionalised PBIs and butylamine-based solvent systems to determine which gave the nicest films (*i.e.*, those that were the most homogenous, and had no obvious defects by eye) (Fig. S1, ESI†). All inks were prepared at a PBI concentration of 0.5 mg mL<sup>-1</sup>, spin-coated onto plasma-cleaned glass substrates and annealed at 100 °C for ten minutes to remove any residual solvent. From these preliminary results, we found that using **PBI-Y** in butylamine alone gave the most uniform films and thus was selected for further study and use in OPV devices.

### Film selection for further study and use in OPV devices

Solutions of **PBI-Y** were prepared at a concentration of 0.5 mg mL<sup>-1</sup> in butylamine and left to stir for 1 hour to ensure dissolution of the PBI. Upon solubilising the **PBI-Y** solution, **PBI-Y** remains soluble indefinitely at room temperature, allowing for coating over longer time periods and at room temperature. Spin-coating and slot-die coating onto plasma-

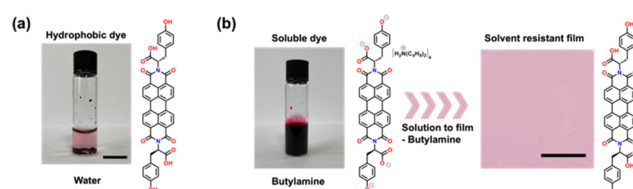


Fig. 2 Green solvent filming process. Chemical structure and photographs of **PBI-Y** studied in (a) water (0.5 mg mL<sup>-1</sup>) and (b) butylamine (0.5 mg mL<sup>-1</sup>) (left) and the resulting spin-coated film on plasma-cleaned glass (right). Scale bar represents 1 cm.



cleaned glass/ITO/SnO<sub>2</sub>-coated glass formed highly uniform thin films at room temperature. These films were thermally annealed at 100 °C for 10 minutes to accelerate the evaporation of residual butylamine.

### PBI-Y film optical and surface characterisation

The optical properties of glass/ITO/SnO<sub>2</sub>/PBI-Y films were studied *via* UV-visible absorption spectroscopy (Fig. 3a). The slot-die coated films showed an increased light absorption compared to the spin-coated films. This increase in intensity could be due to the butylamine evaporating more quickly during slot-die coating, as the printing head and bed were both heated, allowing more material to be deposited on the substrate. This was confirmed using profilometry, with spin-coated films having a thickness of 25 nm and slot-die coated films having a thickness of 32 nm (Fig. S3 and S4, ESI†). However, we note that it was not possible to resolve thickness data for films made at a PBI-Y concentration of 0.5 mg mL<sup>-1</sup>. Therefore, the above data is for films made from a PBI-Y concentration of 5 mg mL<sup>-1</sup>, but we would expect the same trend to be observed at lower concentrations. The peak ratios at 510 and 545 nm (attributed to the 0-0 and 0-1 vibronic bands of the S<sub>0</sub>-S<sub>1</sub> transitions) can determine whether you have H-type of J-type aggregates present in the film.<sup>34,37,38</sup> For both spin- and slot-die coated films, this peak ratio was very similar, suggesting a similar molecular packing of the PBIs regardless of coating method (Fig. 3a). AFM was used to investigate the surface of glass/ITO/SnO<sub>2</sub>/PBI-Y film formation and, consequently, the surface modification of SnO<sub>2</sub> before and after deposition of PBI-Y (Fig. 3b). The root-mean-square (RMS) roughness values of SnO<sub>2</sub>-only films are 1.4 and 1.1 nm for spin-coated and slot-die coated films, respectively. In both films, the presence of PBI-Y leads to a smoother surface, with an RMS value of 1 nm for spin-coated films and 0.9 nm for slot-die coated films.

### PBI-Y film solvent resistance

As previously mentioned, solvent resistance is crucial when developing multi-layered devices. However, forming solvent resistant films of conjugated materials from green solvents is challenging. To test the films' solvent resistance, we exposed the glass/ITO/SnO<sub>2</sub>/PBI-Y films to organic solvents commonly used in orthogonal processing (*o*-xylene, ethanol, and water) (Fig. 4). The films were inspected visually (Fig. 4a), and UV-visible spectra were collected to assess the film quality (Fig. 4b). All films showed no significant dissolution, swelling, cracking or dewetting. Only with water did we observe a slight decrease in the absorption of the film, with those dipped in *o*-xylene and ethanol giving identical spectra to the undipped film. Welch *et al.* have previously reported solvent resistant films from an N-annulated perylene bisimide (PDIN-H).<sup>39</sup> However, these films showed a change in absorption profile upon the addition of *o*-xylene, a common solvent used for processing photoactive layers.<sup>14,40,41</sup> The solvent resistance of the PBI-Y films is likely due to the strong intermolecular hydrogen bonding between the amino acid carboxyl groups of adjacent molecules. Furthermore, the  $\pi$ - $\pi$  stacking plays an important role in inducing more favourable aggregation and decreased solubility, allowing the films to be resistant in both polar and non-polar solvents. When designing solvent-resistant films, it is common for a post-treatment stage to be used postdeposition to generate this resistance.<sup>42</sup> Such methods require either putting energy into the system using heat<sup>43</sup> or UV light<sup>44</sup> or by using chemical reagents.<sup>45</sup> However, here we present a way to make solvent resistant and uniform films without the need for such treatment.

### Spin-coated organic solar cell devices

First, we optimised our OPV devices using spin-coating. A device architecture of glass/ITO/SnO<sub>2</sub>/ETL/PM6:Y6C12/MoO<sub>x</sub>/Ag was utilised to validate the film formation and performance of PBI-Y cathode interlayers in OPVs. We chose PM6/Y6C12 as our photoactive layer as we have previously

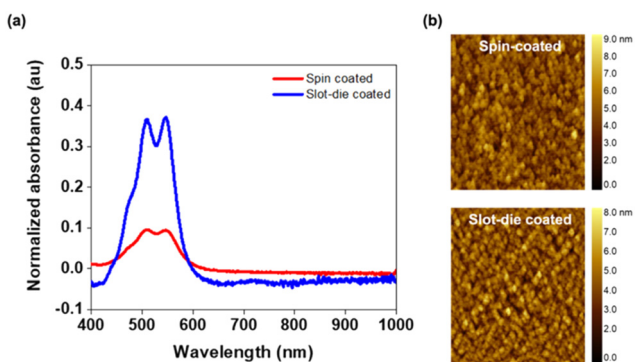


Fig. 3 (a) Absorption spectra of spin-coated and slot-die coated SnO<sub>2</sub>/PBI-Y films. (b) AFM images of spin-coated (top) and slot-die coated (bottom) SnO<sub>2</sub>/PBI-Y films. All films were cast at a concentration of 0.5 mg mL<sup>-1</sup>, in air and at room temperature.

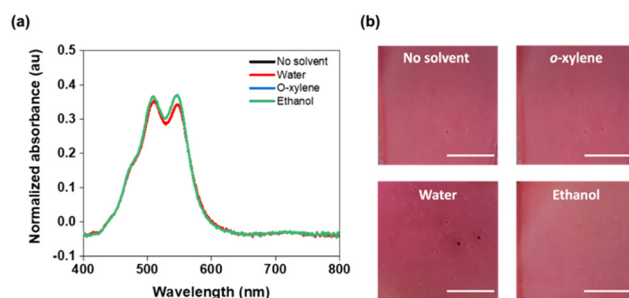


Fig. 4 (a) Optical absorption spectra and (b) photographs of 1.5 cm × 1.5 cm of glass/SnO<sub>2</sub>/PBI-Y films with no solvent and films dipped in water, *o*-xylene and ethanol for 15 seconds and then removed and left to dry. All films were spin-coated at a concentration of 0.5 mg mL<sup>-1</sup>, in air and at room temperature, onto glass substrates. The scale bar represents 1 cm.



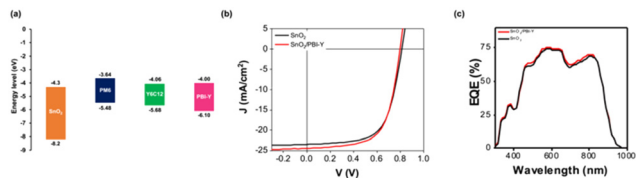


Fig. 5 (a) The energy levels of  $\text{SnO}_2$ , PM6, Y6C12 and PBI-Y. (b)  $J$ - $V$  curves and (c) EQE spectra of spin-coated  $\text{SnO}_2/\text{PBI-Y}$  devices (red) compared to reference with  $\text{SnO}_2$  only (black).

demonstrated slot-die coated PM6:Y6C12 OPV cells with PCE values greater than 10%.<sup>14</sup> Furthermore, this photoactive layer was processed from the non-halogenated solvent, *o*-xylene. Energy-level diagrams of the respective layers and current density-voltage ( $J$ - $V$ ) plots are displayed in Fig. 5 (device metrics are given in Table S4, ESI†). References devices using an  $\text{SnO}_2$  ETL gave a PCE of 12.5%, consistent with the literature.<sup>46,47</sup> Use of an  $\text{SnO}_2/\text{PBI-Y}$  ETL gave a similar, but slightly higher PCE of 12.8%. Furthermore, the  $J_{\text{SC}}$  value for the  $\text{SnO}_2/\text{PBI-Y}$  device was higher than for the reference device ( $J_{\text{SC}}$  values of  $24.5 \text{ mA cm}^{-2}$  and  $23.5 \text{ mA cm}^{-2}$ , respectively). Such results suggest that the PBI-Y is assisting with charge separation of the exciton, resulting in an improved short-circuit current.<sup>35</sup> The external quantum efficiency (EQE) results for spin-coated devices (Fig. 5c) show a broad photoresponse from 400 nm to 900 nm in accordance with their corresponding absorption spectra (Fig. 3a). Moreover, the integrated  $J_{\text{SC}}$  values obtained from the EQE are within 12% mismatch of those obtained from the  $J$ - $V$  measurements ( $20.64 \text{ mA cm}^{-2}$  compared to  $23.31 \text{ mA cm}^{-2}$ ). We also made spin-coated PBI-Y devices using NaOH (0.1 M, aqueous) as our base to compare the device metrics (Fig. S5 and Table S5, ESI†), which gave a lower PCE of 10.3%, a  $J_{\text{SC}}$  of  $23.12 \text{ mA cm}^{-2}$ , and a fill factor (FF) of 57.3%. Overall, these proof-of-concept spin-coated devices demonstrate the use of amine solvent-processed PBI-Y organic films to function as electron transport layers.

### Large-area slot-die coated solar cell devices

As previously discussed, owing to scalability, compatibility with roll-to-roll technology, and low material wastage, slot-die coating has been recognised as a more applicable coating process, particularly on an industrial scale. Therefore, we fabricated OPV devices with all organic layers formed using slot-die coating in ambient conditions. A schematic representation of the slot-die coating process and a picture of the final devices are shown in Fig. 6. All films were coated on glass/ITO substrates in 10 cm strips, which is compatible with small-scale module designs, and is representative of industrial processes using continuous coating.<sup>14</sup> OPV device metrics (average for 10 devices) are given in Table S6, ESI† and  $J$ - $V$  curves are presented in Fig. 6. Devices with  $\text{SnO}_2/\text{PBI-Y}$  ETLs exhibited an average PCE of 10.6%, with a  $J_{\text{SC}}$  of  $22.3 \text{ mA cm}^{-2}$ , an open-circuit voltage ( $V_{\text{OC}}$ ) of 0.78 V, and an FF of 61%. The  $V_{\text{OC}}$  of the slot-die coated devices was slightly

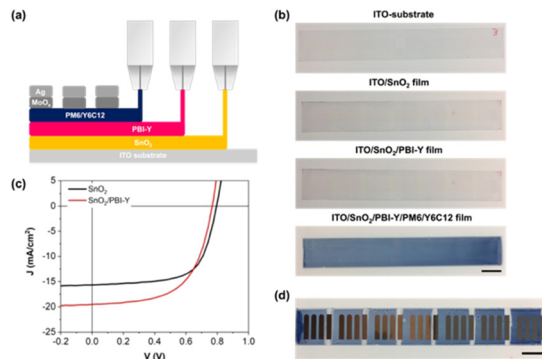


Fig. 6 (a) Schematic diagram representing the slot-die coating process. (b) Camera images of the patterned ITO-coated glass substrate (10 cm strip), and each slot-die coated layer under ambient conditions. The scale bar represents 1 cm. (c)  $J$ - $V$  curves of slot-die coated  $\text{SnO}_2/\text{PBI-Y}$  devices (red) compared to reference with  $\text{SnO}_2$  only (black). (d) Camera image of the slot-die coated device after the silver and  $\text{MoO}_x$  deposition, forming  $0.12 \text{ cm}^2$  active area devices.

lower than the spin-coated devices (0.78 V vs. 0.80 V for spin-coated devices). To the best of our knowledge, there are limited slot-die coated devices using  $\text{SnO}_2$  as the electron transport layer in the literature. However, we have previously made  $\text{SnO}_2/\text{PDIN-H}$  based slot-die coated OPV devices with PCE values of 7.9%.<sup>33</sup> Therefore, this work shows amino acid perylene bisimides have improved device performance than the alkylated derivative.

## Conclusions

In this work, we developed a simple amine solvent processable PBI-based CIL for OPV devices. The AFM, UV-visible absorption spectroscopy and device parameters established PBI-Y as a potential interlayer for  $\text{SnO}_2$  ETLs, which could also apply to other amino acid appended PBIs. The PBI-Y was capable of forming smooth and uniform thin layers using both spin-coating and slot-die coating, suggesting its applicability for use in industrial large-scale device manufacturing. The  $\text{SnO}_2/\text{PBI-Y}$ -based OPVs showed improved device metrics (PCE and  $J_{\text{SC}}$  values) in comparison to pristine  $\text{SnO}_2$ . The processability of amino acid appended PBIs from an amine-based solvent to deliver solvent resistant CIL films opens up new opportunities for high-performance and scalable organic photovoltaics.

## Conflicts of interest

There are no conflicts to declare.

## Acknowledgements

ERD would like to thank the UKRI (MR/V021087/1) and the Royal Society (RGS\R1\231360) for funding. REG would like to thank the UKRI and MITACS UK-Canada Globalink Doctoral Exchange Scheme (NE/X00662X/1) and the EPSRC (EP/R51322/1) for funding. GCW acknowledges funding from the NSERC DG program (2019-04392), the Canada Foundation for



Innovation, the Western Economic Development Fund (now Priorities Economic Development Canada) and the University of Calgary. This research was undertaken thanks in part to funding from the Canada First Research Excellence Fund (CFREF).

## Notes and references

- 1 Y.-W. Su, S.-C. Lan and K.-H. Wei, *Mater. Today*, 2012, **15**, 554–562.
- 2 O. Inganäs, *Adv. Mater.*, 2018, **30**, 1800388.
- 3 V. Pecunia, L. G. Occhipinti and R. L. Z. Hoye, *Adv. Energy Mater.*, 2021, **11**, 2100698.
- 4 F. C. Krebs, N. Espinosa, M. Hösel, R. R. Søndergaard and M. Jørgensen, *Adv. Mater.*, 2014, **26**, 29–39.
- 5 H. Li, S. Liu, X. Wu, S. Yao, X. Hu and Y. Chen, *Energy Environ. Sci.*, 2023, **16**, 76–88.
- 6 M. Jiang, H. Bai, H. Zhi, J. Sun, J. Wang, F. Zhang and Q. An, *ACS Energy Lett.*, 2021, **6**, 2898–2906.
- 7 W. Zhai, A. Tang, B. Xiao, X. Wang, F. Chen and E. Zhou, *Sci. Bull.*, 2018, **63**, 845–852.
- 8 M. E. Farahat and G. C. Welch, *Colorants*, 2023, **2**, 151–178.
- 9 Y. Cui, H. Yao, J. Zhang, K. Xian, T. Zhang, L. Hong, Y. Wang, Y. Xu, K. Ma, C. An, C. He, Z. Wei, F. Gao and J. Hou, *Adv. Mater.*, 2020, **32**, 1908205.
- 10 S. Guo, Y. Hu, M. Qin, J. Li, Y. Wang, J. Qin and P. Cheng, *Mater. Horiz.*, 2022, **9**, 2097–2108.
- 11 Q. He, P. Kafourou, X. Hu and M. Heeney, *SN Appl. Sci.*, 2022, **4**, 247.
- 12 X. Li, H. Yang, X. Du, H. Lin, G. Yang, C. Zheng and S. Tao, *J. Chem. Eng.*, 2023, **452**, 139496.
- 13 M. Yavari, M. Mazloum-Ardakani, S. Gholipour, M. M. Tavakoli, S. H. Turren-Cruz, N. Taghavinia, M. Grätzel, A. Hagfeldt and M. Saliba, *Adv. Energy Mater.*, 2018, **8**, 1800177.
- 14 F. Tintori and G. C. Welch, *Adv. Mater. Interfaces*, 2022, **9**, 2101418.
- 15 M. E. Farahat, A. Laventure, M. A. Anderson, M. Mainville, F. Tintori, M. Leclerc, E. L. Ratcliff and G. C. Welch, *ACS Appl. Mater. Interfaces*, 2020, **12**, 43684–43693.
- 16 Y. Liu, J. Zhang, C. Tian, Y. Shen, T. Wang, H. Zhang, C. He, D. Qiu, Y. Shi and Z. Wei, *Adv. Funct. Mater.*, 2019, **31**, 1805089.
- 17 C. Capello, U. Fischer and K. Hungerbühler, *Green Chem.*, 2007, **9**, 927.
- 18 G. Wang, M. A. Adil, J. Zhang and Z. Wei, *Adv. Mater.*, 2019, **31**, 1805089.
- 19 A. S. Gertsen, M. F. Castro, R. R. Søndergaard and J. W. Andreasen, *Flexible Printed Electron.*, 2020, **5**, 014004.
- 20 L. Wang, J.-Z. Zhan, W.-K. Zhong, L. Zhu, G.-Q. Zhou, T.-Y. Hao, Y.-C. Zou, Z.-H. Wang, G. Wei, Y.-M. Zhang and F. Liu, *Chin. J. Polym. Sci.*, 2023, **41**, 842–850.
- 21 S. Huang, P. Li, J. Wang, J. C.-C. Huang, Q. Xue and N. Fu, *J. Chem. Eng.*, 2022, **439**, 135687.
- 22 G. Kumar and F.-C. Chen, *J. Phys. D: Appl. Phys.*, 2023, **56**, 353001.
- 23 Z. Ghorannevis, E. Akbarnejad and M. Ghorannevis, *J. Theor. Appl. Phys.*, 2015, **9**, 285–290.
- 24 L. Passoni, F. Fumagalli, A. Perego, S. Bellani, P. Mazzolini and F. Di Fonzo, *Nanotechnology*, 2017, **28**, 245603.
- 25 B. Yang, C. Yao, Y. Yu, Z. Li and X. Wang, *Sci. Rep.*, 2017, **7**, 4936.
- 26 Y. Jiang, L. Sun, F. Jiang, C. Xie, L. Hu, X. Dong, F. Qin, T. Liu, L. Hu, X. Jiang and Y. Zhou, *Mater. Horiz.*, 2019, **6**, 1438–1443.
- 27 T. Kong, R. Wang, D. Zheng and J. Yu, *Front. Chem.*, 2021, **7**, 4936.
- 28 X. Zeng, T. Zhou, C. Leng, Z. Zang, M. Wang, W. Hu, X. Tang, S. Lu, L. Fang and M. Zhou, *J. Mater. Chem. A*, 2017, **5**, 17499–17505.
- 29 N. Kudo, Y. Shimazaki, H. Ohkita, M. Ohoka and S. Ito, *Sol. Energy Mater. Sol. Cells*, 2007, **91**, 1243–1247.
- 30 A. A. Said, J. Xie and Q. Zhang, *Small*, 2019, **15**, 1900854.
- 31 D. Görl, X. Zhang and F. Würthner, *Angew. Chem., Int. Ed.*, 2012, **51**, 6328–6348.
- 32 E. R. Draper, J. J. Walsh, T. O. McDonald, M. A. Zwijnenburg, P. J. Cameron, A. J. Cowan and D. J. Adams, *J. Mater. Chem. C*, 2014, **2**, 5570–5575.
- 33 R. Munir, E. Cieplechowicz, R. M. Lamarche, R. Chernikov, S. Trudel and G. C. Welch, *Adv. Mater. Interfaces*, 2022, **9**, 210918.
- 34 D. Görl and F. Würthner, *Angew. Chem., Int. Ed.*, 2016, **55**, 12094–12098.
- 35 J. Cameron, D. J. Adams, P. J. Skabara and E. R. Draper, *J. Mater. Chem. C*, 2022, **10**, 3944–3950.
- 36 E. R. Draper, L. J. Archibald, M. C. Nolan, R. Schweins, M. A. Zwijnenburg, S. Sproules and D. J. Adams, *Chem. – Eur. J.*, 2018, **24**, 4006–4010.
- 37 A. Oleson, T. Zhu, I. S. Dunn, D. Bialas, Y. Bai, W. Zhang, M. Dai, D. R. Reichman, R. Tempelaar, L. Huang and F. C. Spano, *J. Phys. Chem. C*, 2019, **123**, 20567–20578.
- 38 A. G. Smirnov, M. Onuoha, M. S. Bechtel, E. Houser, F. C. Peiris, D. H. Johnston, L. R. Madison and C. M. Mauck, *Vib. Spectrosc.*, 2023, **126**, 103534.
- 39 C. R. Harding, J. Cann, A. Laventure, M. Sadeghianlemraski, M. Abd-Ellah, K. R. Rao, B. S. Gelfand, H. Aziz, L. Kaake, C. Risko and G. C. Welch, *Mater. Horiz.*, 2020, **7**, 2959–2969.
- 40 P. Li, A. Hoff, A. Gasonoo, M. R. Niazi, M. Nazari and G. C. Welch, *Adv. Mater. Interfaces*, 2023, **10**, 2202156.
- 41 S. Zhang, L. Ye, H. Zhang and J. Hou, *Mater. Today*, 2016, **19**, 533–543.
- 42 M. Mooney, C. Crep and S. Rondeau-Gagné, *ACS Appl. Electron. Mater.*, 2022, **4**, 5652–5663.
- 43 Z.-H. Guo, N. Ai, C. R. McBroom, T. Yuan, Y.-H. Lin, M. Roders, C. Zhu, A. L. Ayzner, J. Pei and L. Fang, *Polym. Chem.*, 2016, **7**, 648–655.
- 44 W. Jiang, X. Yu, C. Li, X. Zhang, G. Zhang, Z. Liu and D. Zhang, *Sci. China: Chem.*, 2022, **65**, 1791–1797.
- 45 B. V. Khau, L. R. Savagian, M. De Keersmaecker, M. A. Gonzalez and E. Reichmanis, *ACS Mater. Lett.*, 2019, **1**, 599–605.



- 46 M. R. Niazi, R. Munir, R. M. D'Souza, T. L. Kelly and G. C. Welch, *ACS Appl. Mater. Interfaces*, 2022, **14**, 57055–57063.
- 47 J.-H. Lee, Y.-J. You, M. A. Saeed, S. H. Kim, S.-H. Choi, S. Kim, S. Y. Lee, J.-S. Park and J. W. Shim, *NPG Asia Mater.*, 2021, **13**, 43.

